

Supplementary Material

Boosted Interfacial Charge Dynamics on SnO₂/SnS₂ Heterointerface by Gradient Sulfur Diffusion for Microwaves Absorbing and Electric-thermal Conversion

Zhenkuang Lei ^{a, b, c}, Mingqiang Ning ^{a, c*}, Xueheng Zhuang ^{a, c}, Qikui Man ^{a, b, c*}, Baogen Shen ^{a, c}

^a Key Laboratory of Magnetic Materials and Devices, Ningbo Institute of Materials Technology & Engineering, Chinese Academy of Sciences, Ningbo, Zhejiang, 315201, China

^b College of Materials Science and Opto-Electronic Technology, University of Chinese Academy of Sciences, Beijing, 100049, China

^c Zhejiang Province Key Laboratory of Magnetic Materials and Application Technology, Ningbo Institute of Materials Technology & Engineering, Chinese Academy of Sciences, Ningbo, Zhejiang, 315201, China

(*Corresponding author e-mail: ningmingqiang@nimte.ac.cn; manqk@nimte.ac.cn;

Calculations for electromagnetic absorbing performance

The reflection loss (RL) of absorbers were performed according to the transmission line Equation (1) and (2) as follows^{1,2},

$$Z_{in} = Z_0 \sqrt{\frac{\mu_r}{\epsilon_r}} \tanh \left[j \times \frac{2\pi f d}{c} \sqrt{\mu_r \epsilon_r} \right] \quad (1)$$

$$RL(dB) = 20 \log \left(\frac{Z_{in} - Z_0}{Z_{in} + Z_0} \right) \quad (2)$$

where Z_{in} and Z_0 are input and free space impedance, respectively. μ_0 and ϵ_0 are the complex permeability and complex permittivity of free space. μ and ϵ are the complex permeability and complex permittivity obtained from actual measurement. f is the frequency of microwave, t is the thickness of the absorber, and c is the light speed.

The Debye relaxation formula can describe the relationship between ϵ' and ϵ'' ^{3,4}:

$$\left(\epsilon' - \frac{\epsilon_s + \epsilon_\infty}{2} \right)^2 + (\epsilon'')^2 = \left(\frac{\epsilon_s - \epsilon_\infty}{2} \right)^2 \quad (3)$$

where ϵ_s is the stationary dielectric constant and ϵ_∞ is the dielectric constant at the high-frequency limit.

Furthermore, the dielectric loss can be classified into conduction loss (ϵ_c'') and polarization loss (ϵ_p'') according to Debye theory, and the imaginary part ϵ'' is described as follows: ^{4,5}

$$\epsilon'' = \epsilon_p'' + \epsilon_c'' = \frac{\epsilon_s - \epsilon_\infty}{1 + \omega^2 \tau^2} + \frac{\sigma}{\omega \epsilon_0} \quad (4)$$

Where ϵ_s , ϵ_∞ , ϵ_0 , ω and τ are the static dielectric constant, relative dielectric constant at the high-frequency limit, vacuum permittivity, angular frequency and polarization relaxation time.

The dielectric loss and magnetic loss performance of the absorbers was by using the attenuation constant (α). The α values were calculated as follows⁶:

$$\alpha = \frac{\sqrt{2\pi f}}{c} \sqrt{(\mu_r'' \epsilon_r'' - \mu_r' \epsilon_r') + \sqrt{(\mu_r'' \epsilon_r'' - \mu_r' \epsilon_r')^2 + (\mu_r'' \epsilon_r' + \mu_r' \epsilon_r'')^2}} \quad (5)$$

In several other reports, a delta-function method has been suggested to examine the degree of characteristic impedance matching, as follows^{7,8}:

$$|\Delta| = |\sinh^2(Kfd) - M| \quad (6)$$

$$K = \frac{4\pi}{c} \sqrt{\mu' \varepsilon'} \frac{\sin \frac{\delta_\varepsilon + \delta_\mu}{2}}{\cos \delta_\varepsilon \cos \delta_\mu} \quad (7)$$

$$M = \frac{4\mu' \cos \delta_\varepsilon \varepsilon' \cos \delta_\mu}{(\mu' \cos \delta_\varepsilon - \varepsilon' \cos \delta_\mu)^2 + \left[\tan \left(\frac{\delta_\mu - \delta_\varepsilon}{2} \right) \right]^2 (\mu'' \cos \delta_\varepsilon + \varepsilon'' \cos \delta_\mu)^2} \quad (8)$$

According to previous studies, a smaller $|\Delta|$ value of absorber ($|\Delta| \leq 0.4$) represents better impedance matching^{7,8}.

DFT Calculation

The density functional theory (DFT) is a quantum-mechanical method to study the electronic structure of a many-electron system. Typically, each electron contains three spatial variables, so the multielectron wave function has $3N$ variables (N is the number of electrons). Since the electron density is a function of only three variables, the multielectron wave function problem can be converted to an electron density problem. According to the Kohn-Sham equation, all physical quantities in the non-uniform electron gas model system can be expressed as generalized functions of the ground state electron density⁹:

$$E_i \varphi_i(r) = \left[-\nabla^2 + V_{ext}(r) + \int \frac{n(r')}{|r - r'|} dr' + \frac{\delta E_{xc}[n(r)]}{\delta n(r)} \right] \varphi_i(r) \quad (9)$$

It is generally assumed that the electron density is uniformly distributed, so the uniform electron gas density function can be used to calculate the exchange-correlation energy generalization for non-uniform electron gas by following equation¹⁰:

$$E_{xc}^{LDA}[n(r)] = \int n(r) \varepsilon_{xc}[n(r)] dr \quad (10)$$

Where, $\varepsilon_{xc}[n(r)]$ is the exchange-correlation energy generalization of a

homogeneous electron gas. However, in practice, the electron density is not uniformly distributed. Therefore, the local density approximation is only a rather crude single-electron approximation with poor accuracy. In order to be closer to the actual material system, it is necessary to introduce the generalized gradient approximation (GGA) to exact the exchange the correlation energy functionals accurately as follow¹¹:

$$E_{xc}(n(r)) = \int n(r) \varepsilon_{xc}[n(r)] dr + E_{xc}^{GGA}(n(r), \nabla n(r)) \quad (11)$$

The Vienna ab initio simulation package (VASP) software was used to perform all DFT calculations. The nuclei-electron and the electron exchange correlation interactions were described by the projector augmented wave (PAW) potentials¹² and the GGA¹³. The cut-off energy for plane wave is set to 400 eV. The energy criterion is set to 10–4 eV in iterative solution of the Kohn-Sham equation. A vacuum layer of 10 Å is added perpendicular to the sheet to avoid artificial interaction between periodic images. K-space was sampled with a grid of 5×5×1 under the Monkhorst-Pack scheme due to the supercell. All the structures are relaxed until the residual forces on the atoms have declined to less than 0.03 eV/Å.

Besides, to describe the polarization ability for the four model structures, the dipole moment P was calculated by following equation:

$$P = \int (r - R_{center}) \rho_{ions + valence}(r) d^3r \quad (12)$$

Where R_{center} is the observation sites, and d represents the displacement vector between positive and negative charge^{14–17}. And the electric polarizability could be further calculated by following equation:

$$\sum P/\Delta V = \chi_e \varepsilon_0 E \quad (13)$$

where, ΔV , ε_0 and E represent the volume element, the vacuum permittivity and the electric field, respectively¹⁸.

Finite Element Simulation

The exact sizes numerical models were developed in COMSOL software to study electric field distribution and electric energy loss distribution of absorber by the

limited integral method. Incident microwaves with an excitation power of 1 W from the source are injected into the absorber along the z-axis (x-axis in the direction of magnetic field polarization and y-axis in the direction of electric field polarization). Exactly matched layers are used at the top and bottom of the computational domain to absorb the reflected and transmitted microwaves, respectively. The electromagnetic field in the simulation domain was obtained by solving Maxwell equations in the frequency domain.

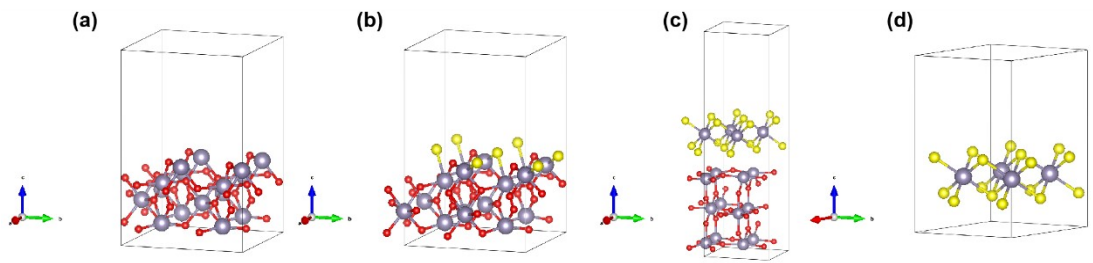


Figure S1. The crystal structure models of (a) S-0, (b) S-1, (c) S-2 and (d) S-3 used for the DFT calculation.

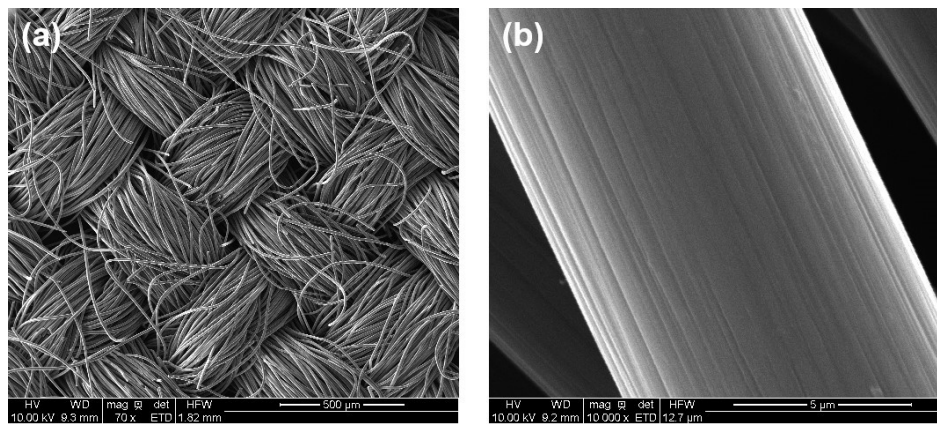


Figure S2. The SEM images of carbon cloth.

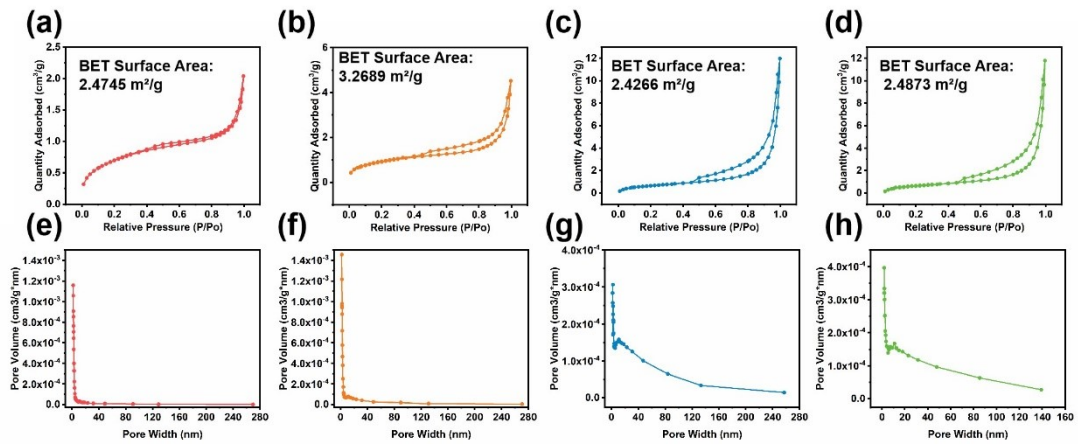


Figure S3. a-d) N_2 adsorption-desorption isothermals and e-h) pore size distributions of all samples.

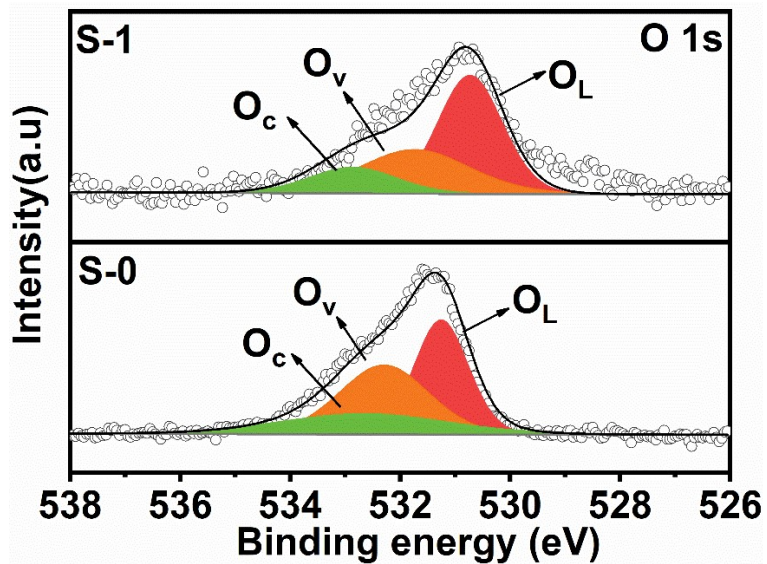


Figure S4. High resolution O 1s spectra of S-0 and S-1

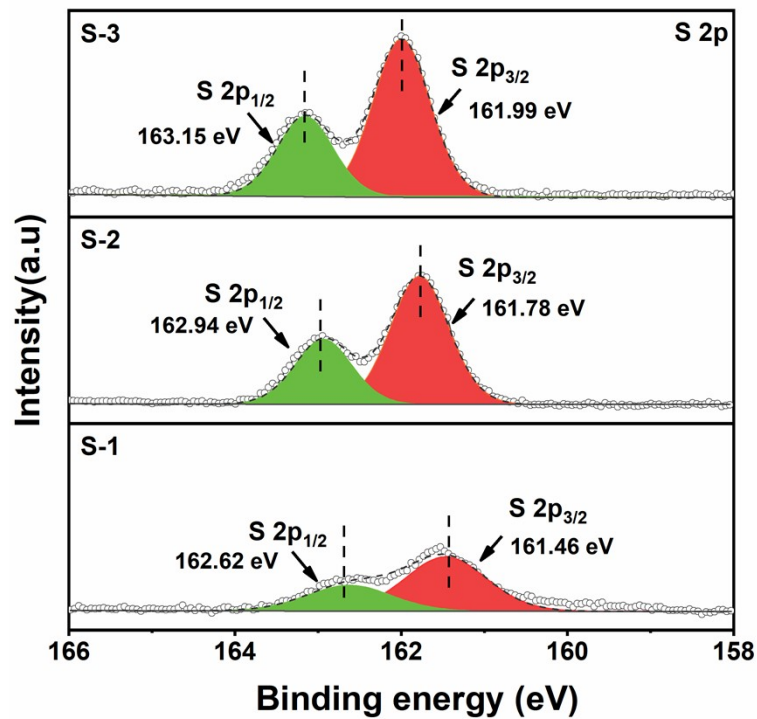


Figure S5. High resolution S 2p spectra of S-1, S-2 and S-3.

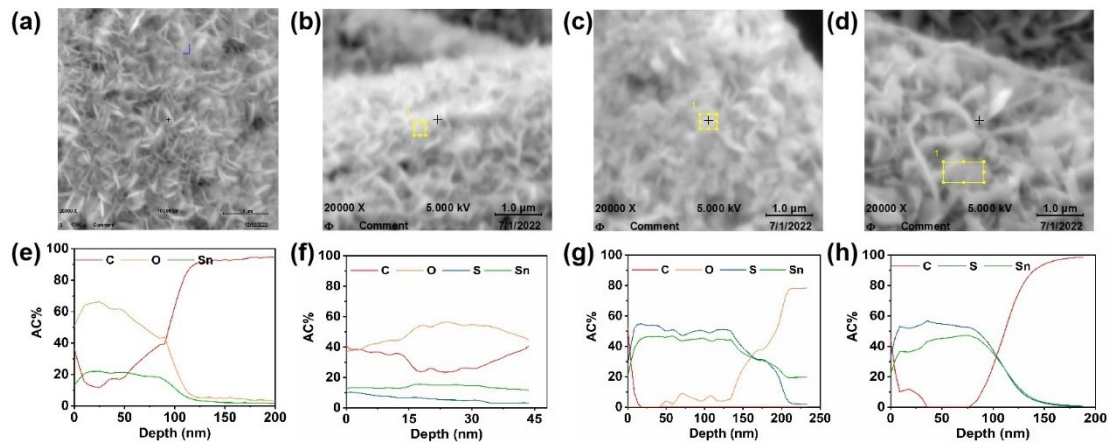


Fig. S6. (a, b, c, d) The digital images and (e, f, g, h) distribution curves of the C, O, S, Sn elements in the vertical direction of S-0, S-1, S-2 and S-3 absorbers.

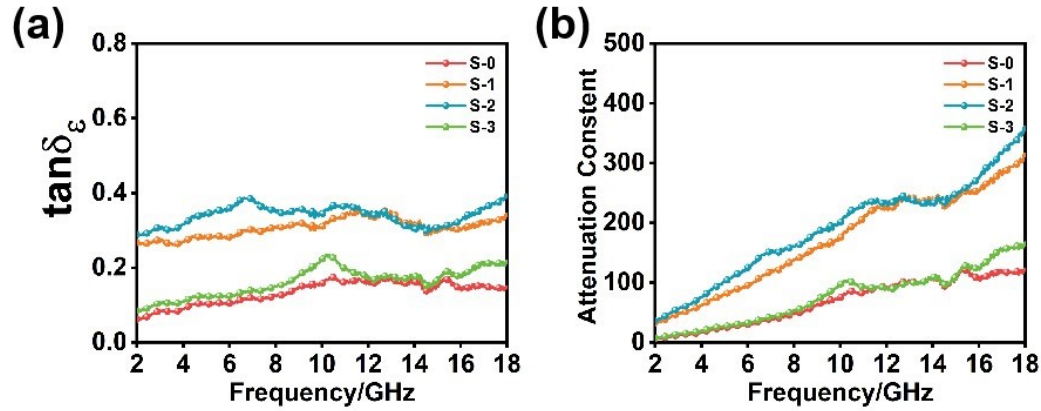


Figure S7. (a) The dielectric loss tangents ($\tan\delta\epsilon$) and (b) attenuation constants (α) of S-0, S-1, S-2 and S-3 absorbers.

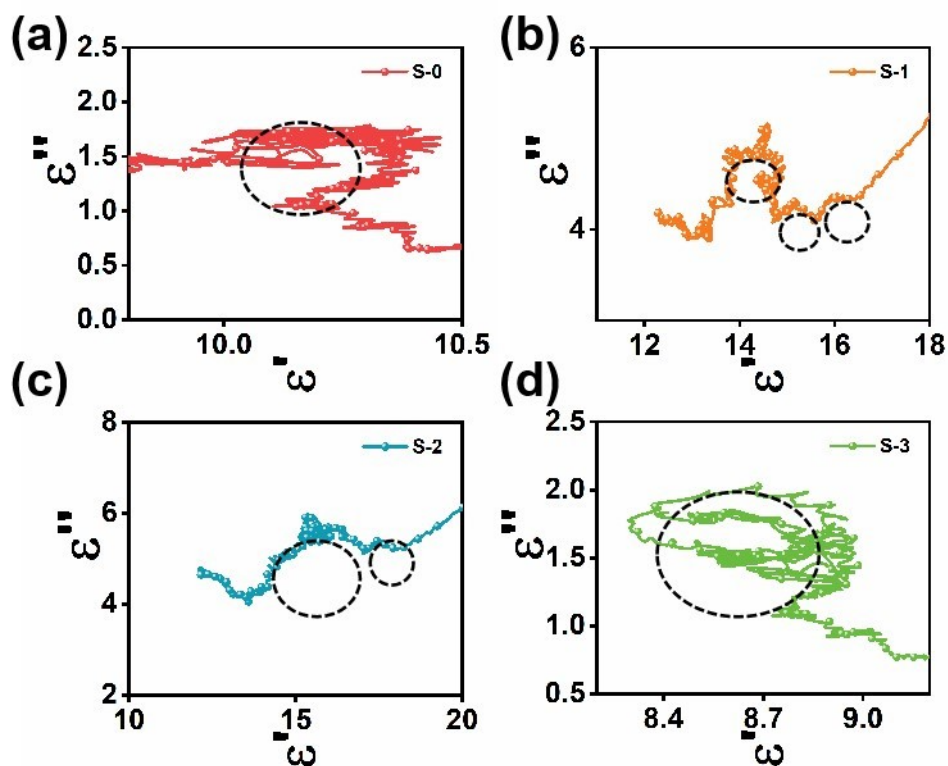


Figure S8. The Cole-Cole curves and enlarge image of **a)** S-0, **b)** S-1, **c)** S-2, and **d)** S-3 absorbers.

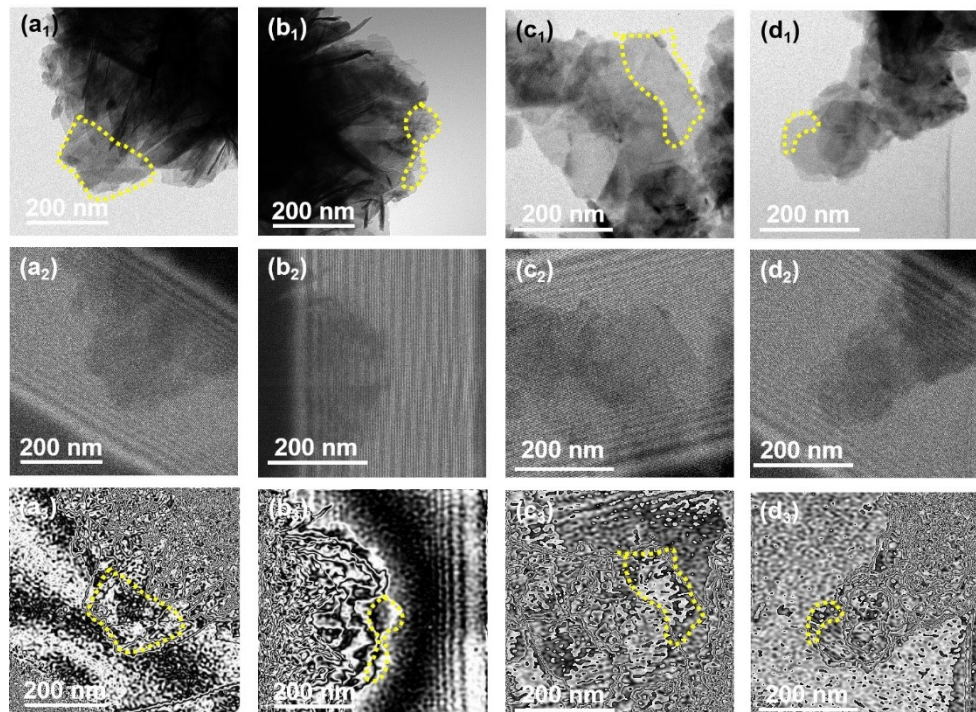


Figure S9. The TEM images and off-axis electron holograms of (a₁-a₃) S-0, (b₁-b₃) S-

1, (c₁-c₃) S-2 and (d₁-d₃) S-3 absorbers.

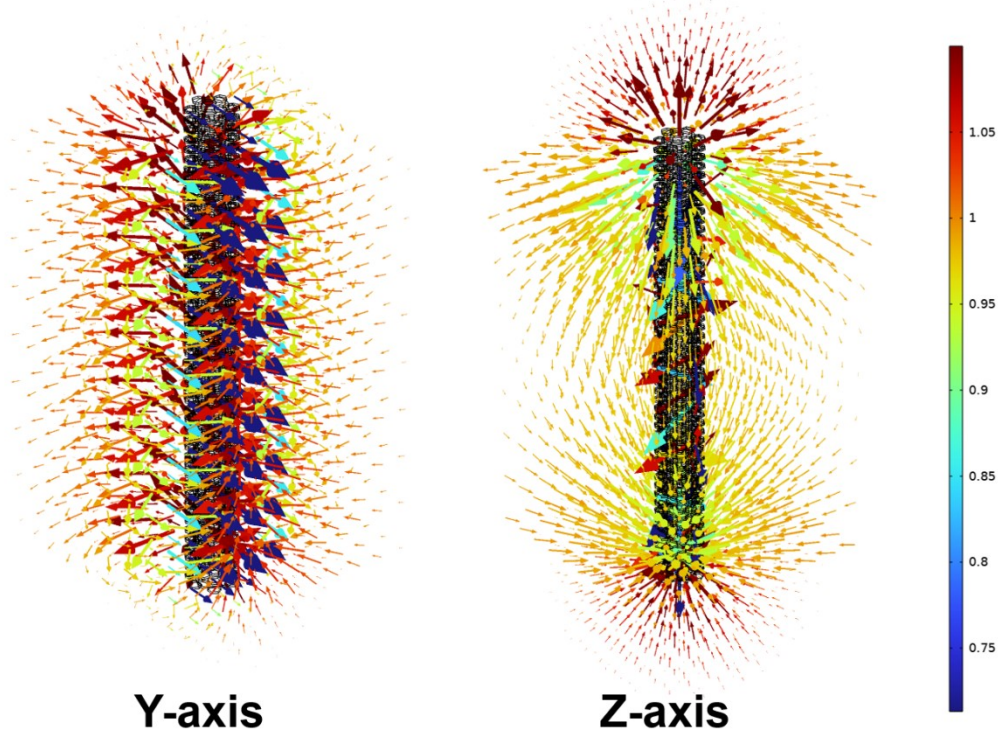


Figure S10. The scattered field distribution of S-2 sample at the incidence of electromagnetic waves from the Y-axis and Z-axis directions

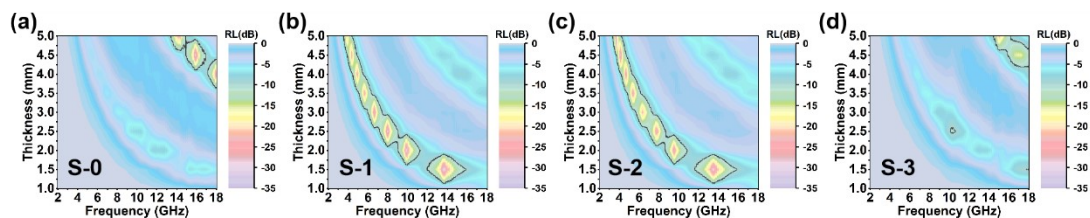


Figure S11. The 2D projection maps of a) S-0, b) S-1, c) S-2, d) S-3.

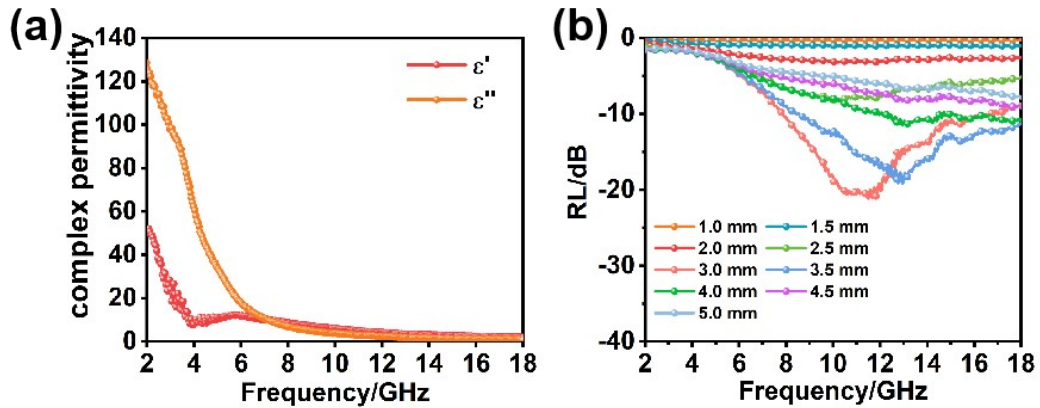


Figure S12. The complex permittivity and reflection loss of pure carbon cloth.

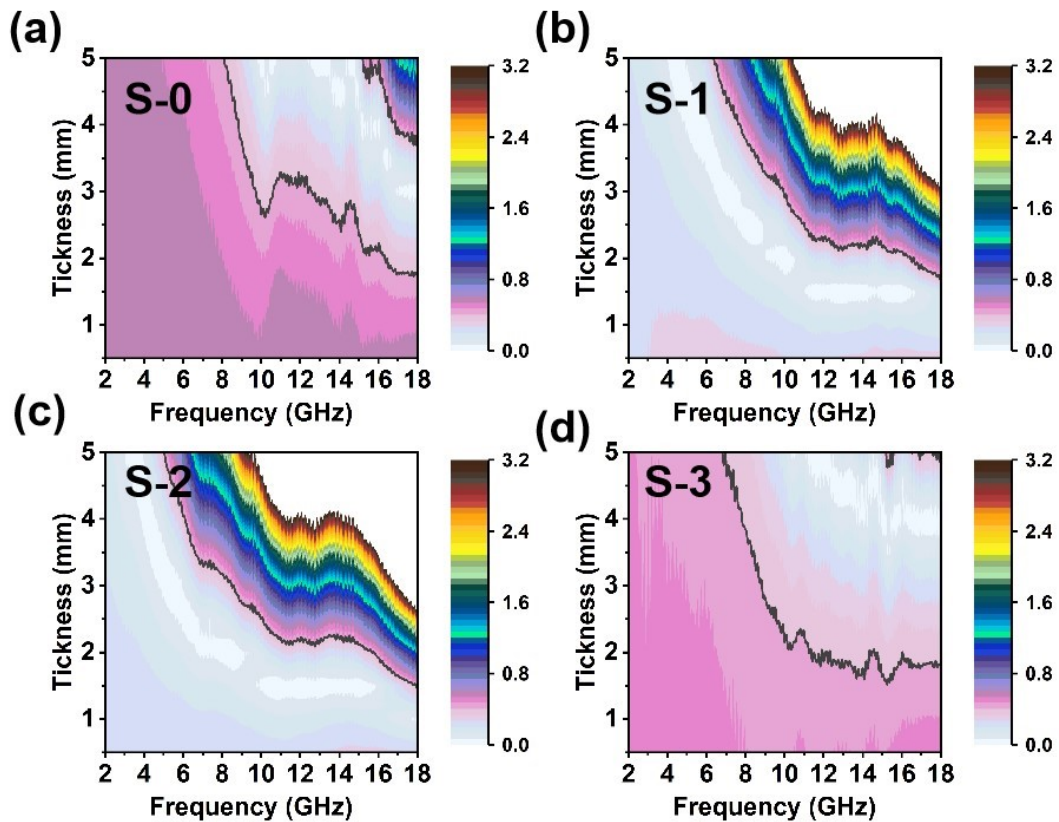


Figure S13. The calculated 2D $|\Delta|_f$ maps of (a) S-0, (b) S-1, (c) S-2, and (d) S-3 absorbers.

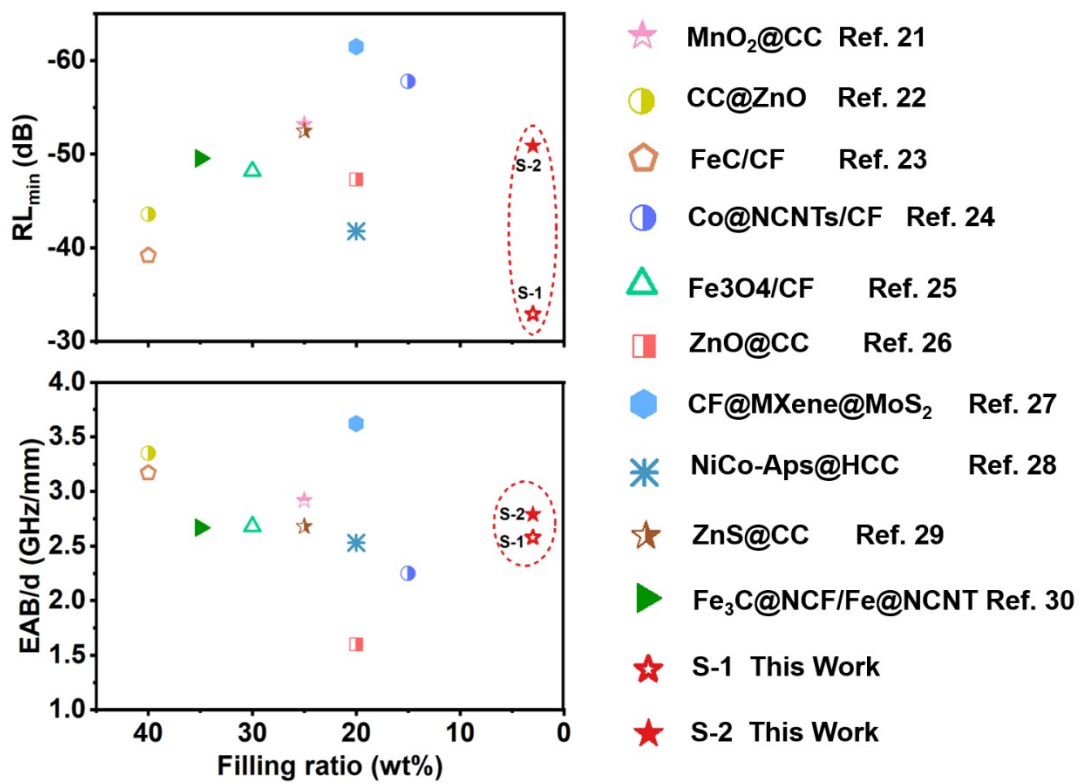


Figure S14. The detailed comparison of EMW absorption performances comparison of typical carbon fiber or carbon cloth based composites in previous researches.

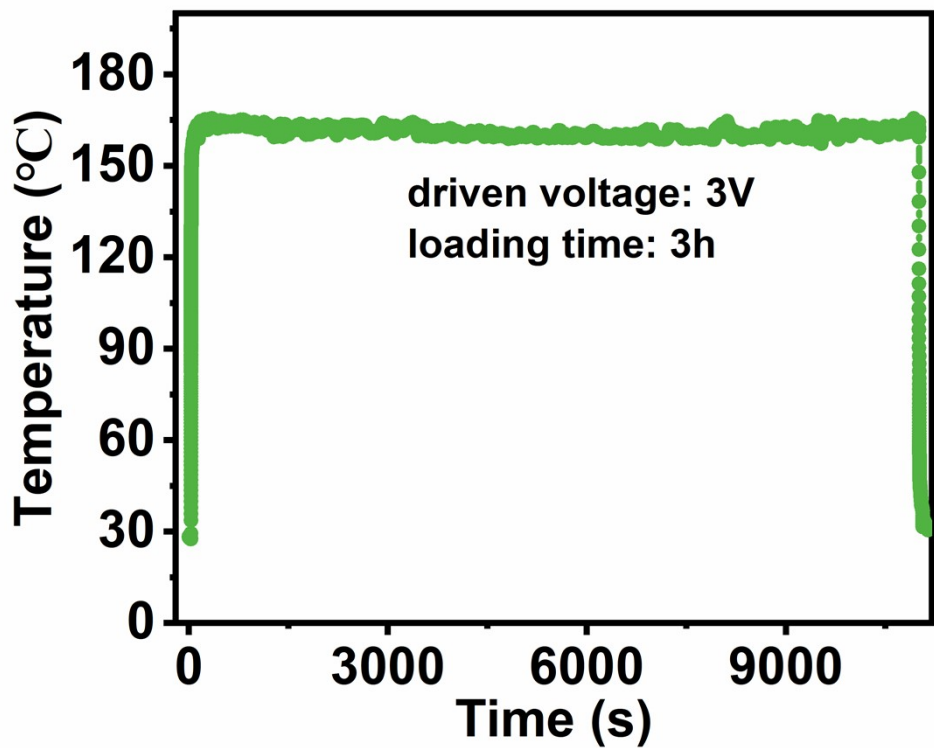


Figure S15. The long-term temperature-time curve at 3V driven voltages of S-2 sample

Table S1. The calculated dipole moment and polarization

Samples	Dipole moment ($e\cdot\text{\AA}$)	Polarization (C/m ²)
S-0	-0.481535	-0.192961779
S-1	-13.300412	-0.466408238
S-2	-25.131208	-0.679365423
S-3	-0.000521	-0.000595551

Table S2. The EMW absorption performances of typical carbon fiber or carbon cloth based composites in previous researches and this work.

Sample	RLmin (dB)	EAB (GHz)	Thickness (mm)	Filler loading ratio (wt%)	Ref
MnO ₂ @CC	-53.2	5.84	2.0	25	19
CC@ZnO	-43.6	6.7	2	40	20
FeC/CF	-39.2	4.44	1.4	40	21
Co@NCNTs/CF	57.8	4.5	2.0	15	22
Fe ₃ O ₄ /CF	-48.2	5.1	1.9	30	23
ZnO@CC	-47.3	4.0	2.5	20	24
CF@MXene@MoS ₂	-61.51	7.6	3.5 & 2.1	20	25
NiCo-APs@HCC	-41.8	5.8	2.29	20	26
ZnS@CC	-52.5	5.1	1.9	25	27
Fe ₃ C@NCF/Fe@NCNT	-49.56	4	1.5	35	28

S-1	-32.95	3.87	1.5	3	This work
S-2	-50.9	4.18	5&1.5	3	This work

Reference

1. M. Ning, Z. Lei, G. Tan, Q. Man, J. Li and R.-W. Li, *ACS Appl. Mater. Interfaces*, 2021, **13**, 47061–47071.
2. J. Luo, H. Guo, J. Zhou, F. Guo, G. Liu, G. Hao and W. Jiang, *Chem. Eng. J.*, 2022, **429**, 132238.
3. H. Lv, C. Wu, J. Tang, H. Du, F. Qin, H. Peng and M. Yan, *Chem. Eng. J.*, 2021, **411**, 128445.
4. Y. Zhu, J. Li, X. Li, P. Chen and B. Zhu, *J. Alloys Compd.*, 2022, **924**, 166461.
5. H. Xu, G. Zhang, Y. Wang, M. Ning, B. Ouyang, Y. Zhao, Y. Huang and P. Liu, *Nano-Micro Lett.*, 2022, **14**, 102.
6. H.-Y. Wang, X.-B. Sun, S.-H. Yang, P.-Y. Zhao, X.-J. Zhang, G.-S. Wang and Y. Huang, *Nano-Micro Lett.*, 2021, **13**, 206.
7. Y. Gao, L. Pan, Q. Wu, X. Zhuang, G. Tan and Q. Man, *J. Alloys Compd.*, 2022, **915**, 165405.
8. D. Ding, Y. Wang, X. Li, R. Qiang, P. Xu, W. Chu, X. Han and Y. Du, *Carbon*, 2017, **111**, 722–732.
9. K. Luo, V. V. Karasiev and S. B. Trickey, *Phys. Rev. B*, 2018, **98**, 041111.
10. D. Mejia-Rodriguez and S. B. Trickey, *Phys. Rev. A*, 2017, **96**, 052512.
11. P. Verma and D. G. Truhlar, *J. Phys. Chem. Lett.*, 2017, **8**, 380–387.
12. P. Blochl, *Phys. Rev. B*, 1994, **50**, 17953–17979.
13. J. P. Perdew, M. Ernzerhof and K. Burke, *J. Chem. Phys.*, 1996, **105**, 9982–9985.
14. J.-P. Chen, Y.-F. Du, Z.-F. Wang, L.-L. Liang, H. Jia, Z. Liu, L.-J. Xie, S.-C. Zhang and C.-M. Chen, *Carbon*, 2021, **175**, 11–19.
15. Z.-W. Zhao, Q.-Q. Pan, Y.-C. Duan, Y. Wu, Y. Geng, S.-X. Wu and Z.-M. Su, *J. Phys. Chem. C*, 2019, **123**, 6407–6415.
16. M. Li, L. Kou, L. Diao, Q. Zhang, Z. Li, Q. Wu, W. Lu, D. Pan and Z. Wei, *J. Phys. Chem. C*, 2015, **119**, 9782–9790.
17. W. E. Ford, D. Gao, N. Knorr, R. Wirtz, F. Scholz, Z. Karipidou, K. Ogasawara, S. Rosselli, V. Rodin, G. Nelles and F. von Wrochem, *ACS Nano*, 2014, **8**, 9173–

18. J. Xu, L. Liu, X. Zhang, B. Li, C. Zhu, S. Chou and Y. Chen, *Chem. Eng. J.*, 2021, **425**, 131700.
19. X. Li, L. Wang, W. You, L. Xing, L. Yang, X. Yu, J. Zhang, Y. Li and R. Che, *Nanoscale*, 2019, **11**, 13269–13281.
20. L. Wang, X. Li, Q. Li, X. Yu, Y. Zhao, J. Zhang, M. Wang and R. Che, *Small*, 2019, **15**, 1900900.
21. J. Chen, J. Zheng, F. Wang, Q. Huang and G. Ji, *Carbon*, 2021, **174**, 509–517.
22. X. Zhang, M. Liu, J. Xu, Q. Ouyang, C. Zhu, X. Zhang, X. Zhang and Y. Chen, *Chem. Eng. J.*, 2021, 133794.
23. Y. Liu, Z. Chen, W. Xie, S. Song, Y. Zhang and L. Dong, *ACS Sustainable Chem. Eng.*, 2019, **7**, 5318–5328.
24. X. Han, Y. Huang, J. Wang, G. Zhang, T. Li and P. Liu, *Composites Part B: Engineering*, 2022, **229**, 109458.
25. J. Wang, L. Liu, S. Jiao, K. Ma, J. Lv and J. Yang, *Adv. Funct. Mater.*, 2020, **30**, 2002595.
26. Z. Chen, K. Tian, C. Zhang, R. Shu, J. Zhu, Y. Liu, Y. Huang and X. Liu, *J. Colloid Interface Sci.*, 2022, **616**, 823–833.
27. J. Ding, K. Song, C. Gong, C. Wang, Y. Guo, C. Shi and F. He, *J. Colloid Interface Sci.*, 2022, **607**, 1287–1299.
28. H. Xu, B. Li, X. Jiang, Y. Shi, X. Zhang, C. Zhu, X. Zhang and Y. Chen, *Carbon*, 2023, **201**, 234–243.